RESEARCH ARTICLE

Key Points:
- We tested the dynamic equilibrium theory using a hybrid-type model
- Background sediment concentration determines the uniform bed shear stress in equilibrium theory
- Tidal-averaged diffusion coefficient needs calibration in realistic morphodynamic modeling

Correspondence to:
Z. Hu,
zhan.hu@tudelft.nl

Predicting long-term and short-term tidal flat morphodynamics using a dynamic equilibrium theory

Zhan Hu[1,2], Zheng Bing Wang[1,3], Tjerk J. Zitman[1], Marcel J. F. Stive[1], and Tjeerd J. Bouma[2]

[1]Hydraulic Engineering Department, Delft University of Technology, Delft, Netherlands, [2]Spatial Ecology Department, Royal Netherlands Institute for Sea Research, Yerseke, Netherlands, [3]Deltares, Delft, Netherlands

Abstract Dynamic equilibrium theory is a fruitful concept, which we use to systematically explain the tidal flat morphodynamic response to tidal currents, wind waves, sediment supply, and other sedimentological drivers. This theory stems from a simple analytical model that derives the tide- or wave-dominated tidal flat morphology by assuming that morphological equilibrium is associated with uniform bed shear stress distribution. Many studies based on observation and process-based modeling tend to agree with this analytical model. However, a uniform bed shear stress rarely exists on actual or modeled tidal flats, and the analytical model cannot handle the spatially and temporally varying bed shear stress. In the present study, we develop a model based on the dynamic equilibrium theory and its core assumption. Different from the static analytical model, our model explicitly accounts for the spatiotemporal bed shear stress variations for tidal flat dynamic prediction. To test our model and the embedded theory, we apply the model for both long-term and short-term morphological predictions. The long-term modeling is evaluated qualitatively against previous process-based modeling. The short-term modeling is evaluated quantitatively against high-resolution bed-level monitoring data obtained from a tidal flat in Netherlands. The model results show good performances in both qualitative and quantitative tests, indicating the validity of the dynamic equilibrium theory. Thus, this model provides a valuable tool to enhance our understanding of the tidal flat morphodynamics and to apply the dynamic equilibrium theory for realistic morphological predictions.

1. Introduction

Knowledge of tidal flat morphological evolution is of great importance as it is essential to the long-term sustainability of the intertidal ecosystem and related coastal defense values [*Kirwan and Megonigal*, 2013; *Temmerman et al.*, 2013; *Bouma et al.*, 2014]. Furthermore, the short-term sediment dynamic patterns can influence the opportunity for salt marsh or mangroves plants to (re)establish on the bare tidal flat [*Balke et al.*, 2011, 2014], which is important for coastal wetland conservation and restoration.

The complex sedimentary mechanisms in the intertidal environments have been studied by observations [*Fan et al.*, 2006; *Green*, 2011; *Zhu et al.*, 2014], analytical solutions [*Friedrichs and Aubrey*, 1996; *Friedrichs*, 2011], and numerical modeling [*Roberts et al.*, 2000; *Pritchard et al.*, 2002; *Mariotti and Fagherazzi*, 2010; *Hunt et al.*, 2015]. Especially, the analytical model of *Friedrichs and Aubrey* [1996] is a key advancement illustrating the relationship between prevailing hydrodynamic conditions and tidal flat equilibrium bathymetry. In the analytical model, it is assumed that when a tidal flat is in equilibrium, the maximum bed shear stress in a tidal cycle is uniform in space, which leads to zero net sediment transport [*Friedrichs and Aubrey*, 1996]. Based on this idealization, it is found that in tide-dominated conditions the equilibrium tidal flat has a convex-up shape, whereas in wave-dominated conditions the equilibrium tidal flat has a concave-up shape.

Building on the analytical solution, *Friedrichs* [2011] further formulated a dynamic equilibrium concept. It elucidates that observed tidal flat morphology approximates a dynamic equilibrium over annual and longer time scales, which is somewhere in between purely tide-dominated (convex) and purely wave-dominated (concave) extremes. On a shorter time scale, however, tidal flat morphology may deviate from that dynamic equilibrium and approach one or the other extreme depending on the prevailing forcing condition. The dynamic equilibrium theory clarifies the seemingly conflict between the idealized morphological equilibrium state with uniform bed shear stress and the reality with spatially and temporally varying bed shear stress. Tidal flats may be close or far away from their corresponding equilibrium depending on the circumstances.

Tidal flats that stay statically in equilibrium are in fact exceptional [*Pritchard et al.*, 2002; *Tambroni and Seminara*, 2012; *Lanzoni and D'Alpaos*, 2015; Maan et al., submitted]. Besides hydrodynamic forces, tidal flat equilibrium also responds to other drivers acting on various time scales, e.g., external sediment supply changes, bioturbation/bioaggregation, and human interference [*Friedrichs*, 2011; *Green and Coco*, 2014; *Corenblit et al.*, 2011; *Murray et al.*, 2008].

A number of observations and modeling studies have shown that large-scale long-term tidal flat morphology generally agrees with the analytical model and the dynamic equilibrium theory [*Kirby*, 2000; *Bearman et al.*, 2010; *Friedrichs*, 2011; *van der Wegen and Jaffe*, 2014]. However, these assessments based on comparing the observed or modeled profile morphology with the static equilibrium profiles derived by the analytical model are largely empirical and indirect. It is because that the analytical model can only handle the idealized state with uniform bed shear stress, but it cannot handle natural conditions with varying bed shear stress. For instance, tidal flat equilibrium in tide-dominated conditions is often defined as the state when a constant (convex-up) cross-shore profile has been reached [*Le Hir et al.*, 2000; *Pritchard et al.*, 2002; *Pritchard and Hogg*, 2003; *Liu et al.*, 2011]. On such a profile, however, the maximum bed shear stress is in fact only uniform in the subtidal area and it decreases to zero in the intertidal area as the inundation depth reduces [*Le Hir et al.*, 2000; *Pritchard et al.*, 2002; *Pritchard and Hogg*, 2003; *Liu et al.*, 2011]. Hence, such an equilibrium is actually not static. The complete tidal flat profile continuously migrates seaward as a constant morphological reaction to the environment that favors sedimentation [*Pritchard et al.*, 2002; *Waeles et al.*, 2004; *Liu et al.*, 2011]. The dynamic morphological behavior with spatially and temporally varying bed shear stress cannot be explained by the static analytical model.

In this study, we develop a model called dynamic equilibrium theory-ESTMORF (DET-ESTMORF), which is a modification of ESTMORF models [*Wang et al.*, 1998, 2008; *Stive et al.*, 1998; *Stive and Wang*, 2003; *Wang and Townend*, 2012]. The most important feature of the DET-ESTMORF model is that it implements the dynamic equilibrium theory and explicitly accounts for the spatiotemporal bed shear stress variations to predict tidal flat morphodynamics. Following the dynamic equilibrium theory, this model defines idealized tidal flat morphological equilibrium as the state with a uniform bed shear stress distribution. The deviation between the uniform bed shear stress (associated with tidal flat equilibrium) and the actual bed shear stress is then the driver of morphological changes. This feature enables the DET-ESTMORF model to apply the dynamic equilibrium theory and derive tidal flat morphodynamics under the conditions with spatiotemporally varying bed shear stress, which is not possible for the static analytical model [*Friedrichs and Aubrey*, 1996].

The aim of this study is (1) to directly test the dynamic equilibrium theory under the condition with spatially and temporally varying forces by evaluating the DET-ESTMORF model and (2) to show how this theory can be applied to predict tidal flat morphodynamics. To evaluate the model, we first compare the long-term tidal flat morphological modeling with the previous process-based model results [e.g., *Roberts et al.*, 2000; *Pritchard et al.*, 2002; *Liu et al.*, 2011]. The process-based models were developed without explicitly including the dynamic equilibrium theory. Thus, the comparison between the DET-ESTMORF and process-based models can be an independent test of the theory. Second, we tested the model quantitatively by calibrating and validating it against high-frequency bed-level monitoring data obtained on a tidal flat in Westerschelde Estuary, Netherlands. In the same process of the model testing, we demonstrate how the dynamic equilibrium concept can be applied for long-term and short-term bed-level change predictions.

2. Method

2.1. DET-ESTMORF Model Description

Both the original ESTMORF model and the DET-ESTMORF model are hybrid-type morphological models. They combine physical process (hydrodynamics and sediment transport) simulations with morphological equilibrium relations to obtain an optimal description of morphological evolutions (Figure 1). This differs from fully process-based models (e.g., Delft3D [*Lesser et al.*, 2004]) that predict sediment dynamics purely by elaborating physical processes (e.g., mass and momentum conservation) without explicitly using equilibrium relations. More specifically, the main difference between these two types of model is in the method of determining local equilibrium concentration field (c_e) (Figure 1). The ESTMORF-type models make use of a morphological equilibrium relation to derive c_e of each element, whereas process-based models derive it directly.
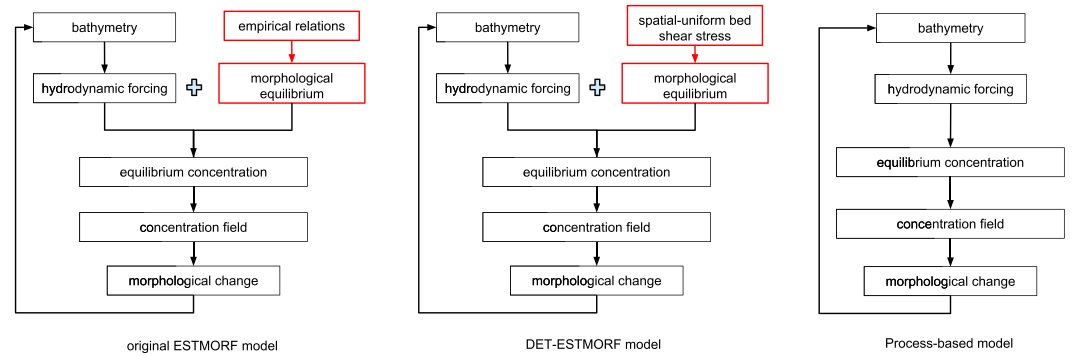
Figure 1. Computational procedure of the (left) original ESTMORF model, (middle) DET-ESTMORF model, and (right) process-based model. The ESTMORF-type models make use of morphological equilibrium relation to derive morphological changes, whereas the process-based models derive morphological changes directly without using equilibrium relations. Different from the original ESTMORF model, the DET-ESTMORF model does not rely on empirical relations to derive the morphological equilibrium but follows the dynamic equilibrium theory and defines the equilibrium as the state with spatially uniform bed shear stress [*Friedrichs and Aubrey*, 1996].

The original ESTMORF model has been successfully applied to predict long-term (decades) morphological evolution of estuaries and tidal lagoons [*Stive et al.*, 1998; *Wang et al.*, 1998, 2008; *Wang and Townend*, 2012]. The same modeling philosophy and approach of ESTMORF models have also been adapted in a more aggregated model called ASMITA (Aggregated Scale Morphological Interaction between Tidal basin and the Adjacent coast) [*Van Goor et al.*, 2003; *Kragtwijk et al.*, 2004; *Dissanayake et al.*, 2011; *Rossington et al.*, 2011]. The morphological equilibrium states in these models were given by empirical relations, e.g., a relation between tidal channel cross-section area with tidal prism volume (e.g., equation (8) in *Wang and Townend* [2012]). To test the dynamic equilibrium theory, we define the tidal flat morphological equilibrium in the DET-ESTMORF model as the state with a spatial-uniform bed shear stress (τ_e), whereas the modeling philosophy and procedures are kept the same as the original ESTMORF model [*Wang et al.*, 1998, 2008; *Stive et al.*, 1998; *Stive and Wang*, 2003; *Wang and Townend*, 2012]. Similar to original ESTMORF models, the DET-ESTMORF model quantifies tidal flat morphological changes over an entire tidal cycle and does not simulate the morphodynamics in different tidal phase.

The philosophy of the DET-ESTMORF models is as follow: sediment is assumed transported only in suspension. If all elements (e.g., from element number *1* to number *k* on the *x* axis of Figure 2) in a morphological system are in equilibrium with uniform τ_E, there is no net sedimentation or erosion anywhere in the system. In an equilibrium state, the sediment concentration is equal to c_E everywhere in the system, which is defined as an overall equilibrium concentration. For each element in the system, a local equilibrium concentration c_e is defined based on the local bed shear stress conditions. If the local bed shear stress is higher than τ_E, then a tendency of erosion exists for this element (Figure 2a), and c_e is higher than c_E. It means that this element demands higher sediment concentration than the average level (i.e., c_E) in order to prevent erosion (or to initiate sedimentation). If the local bed shear stress is lower than τ_E, then a tendency of sedimentation exists for this element (Figure 2a), and c_e is lower than c_E. It means that this element demands lower sediment concentration than c_E in order to prevent erosion (or to initiate sedimentation). In summary, the deviation between τ_E and the actual bed shear stress leads to the tendency of the morphodynamic changes, which is expressed by the distribution of c_e. However, the erosion or sedimentation may not necessarily occur in an element with the corresponding tendency as the morphological changes also depend on the actual sediment availability. For instance, if an element has a tendency of erosion but there is enough sediment available to prevent erosion, the erosion may not occur in the element. Similarly to the process-based models, the actual sediment availability (sediment concentration field) is governed by a diffusion equation. Local morphological changes occur when the actual suspended sediment concentration (c) of an element deviates from its local equilibrium value (c_e). Erosion occurs when c is smaller than c_e; i.e., the actual local sediment concentration is not high enough to prevent erosion (Figure 2b). Conversely, sedimentation occurs if c is larger than c_e; i.e., the actual local sediment concentration is higher than necessary to prevent erosion (or to initiate sedimentation).
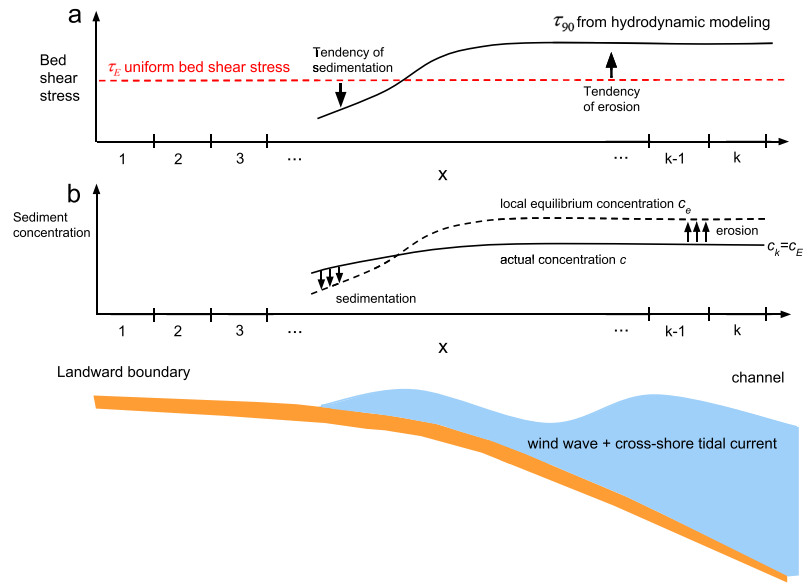
Figure 2. The schematization of the DET-ESTMORF model. The total number of elements in the model is 'k.' From the landward boundary toward the seaward boundary, the element number increases from '1' to 'k.' (a) Spatial bed shear stress distribution determines the corresponding morphological evolution tendency. Following the dynamic equilibrium theory, a uniform bed shear stress is defined as τ_E. The representative hydrodynamic forcing is choosing as the 90th percentile bed shear stress in a tidal cycle (τ_{90}). (b) Variations between τ_E and τ_{90} lead to the morphodynamic tendencies, which determine the distribution of local equilibrium concentration c_E. The actual sediment concentration field (c) is determined by a sediment transport function, with the concentration at the seaward boundary (c_k) being the overall equilibrium concentration (c_E). The deviation between c and c_e determines the actual morphological changes.

For the sediment concentration field quantification of both long-term and short-term modeling, the boundary conditions can be prescribed as following. It is assumed that the outside world of the tidal flat is always in a state of equilibrium and the morphological development of the tidal flat does not affect the sediment availability from the channel (Figure 2b). Therefore, at the seaward boundary the sediment concentration is fixed as c_E (i.e., $c_k = c_E$ in Figure 2, where c_k is the concentration of the most seaward element) acting as a time-invariant boundary condition for long-term tidal flat morphological evolution [e.g., *Van Goor et al.*, 2003; *Wang and Townend*, 2012]. For the landward boundary, however, the condition (c_1) varies depending on the applications and will be specified in section 2.3.

It is noted that most tidal flats in reality are not in a static equilibrium, but they are constantly adapting their morphology around equilibrium [*Friedrichs*, 2011]. Hence, the uniform bed shear stress distribution (τ_E) is generally an idealized state that may not occur in reality. As both τ_E and c_E are related to the idealized equilibrium state and are both uniform on equilibrium tidal flats, τ_E is defined as the bed shear stress that can maintain the constant overall sediment concentration (c_E) in the water column to prevent exchange of sediment with the seabed. Hence, in equilibrium states, the vertical sediment erosion flux balances the vertical deposition flux, which is similar to the process-based model descriptions [*Winterwerp and Van Kesteren*, 2004; *Amoudry and Souza*, 2011]:

$$m_e\left(\frac{\tau_E}{\tau_{cr}} - 1\right) = c_E w_s \tag{1}$$

where m_e is the erosion coefficient [kg/(m^{2}s)] and τ_{cr} is the critical shear stress for erosion (Pa). The used values of m_e and τ_{cr} are listed in Table 1. In the original ESTMORF models for tidal channel modeling [*Wang et al.*, 1998, 2008; *Wang and Townend*, 2012], the local equilibrium concentration c_e is defined based on the ratio between the actual tidal channel cross-sectional area (A) to the equilibrium cross-sectional area (A_E): $c_e = c_E \left(A_E / A\right)^n$, in which A_E is obtained from empirical tidal prism relations and n is defined in Table 1. Thus, c_e is determined based on the comparison between the actual condition and the corresponding equilibrium condition. Following the concept and the formulation in the original ESTMORF

Table 1. Parameters Definition and Values for Morphological Modeling[a]

Parameter	Description	Value	Reference
n	power in equation (2) for the local equilibrium sediment concentration (-)	2	*Wang et al.* [2008]
D	tide-averaged diffusion coefficient (m^2/s), representing the horizontal mixing process by water motion in a tidal cycle	600	*Wang et al.* [2008]
w_s	settling velocity for suspended sediment (m/s)	0.0005	*Roberts et al.* [2000] and *Liu et al.* [2011]
m_e	erosion coefficient [kg/(m^{2}s)]	0.00005	*Roberts et al.* [2000]
p	seabed porosity (-)	0.4	*Liu et al.* [2011]
ρ_s	sediment density (kg/m^3)	2650	*Van Rijn* [2007a]
ρ	water density (kg/m^3)	1000	-
τ_{cr}	critical bed shear stress for erosion (Pa)	0.15	*Roberts et al.* [2000]
f_c	constant friction factor for currents (-)	0.002	*Roberts et al.* [2000]
v	kinematic viscosity coefficient (m^2/s)	0.000001	-

[a]This list provides the setting for the long-term morphological modeling, whereas for the short-term morphological modeling some of the settings are different, which are specified in section 2.3.2.

models [*Wang et al.*, 1998, 2008; *Wang and Townend*, 2012], c_e in DET-ESTMORF is defined based on the ratio between the actual bed shear stress to τ_E as

$$c_e = c_E \left(\frac{\tau_{90}}{\tau_E} \right)^n \tag{2}$$

where τ_{90} is the 90th percentile bed shear stress in a tidal cycle, which accounts for both the characteristic magnitude of energetic forcing as well as the fraction of time that the forcing is strong. This value is chosen in analogy to the 90th percentile velocity of tidal current or wave orbital motion in a tidal cycle, which is a useful scale for evaluating coastal morphology [*Friedrichs and Wright*, 2004; *Friedrichs*, 2011]. n is defined in Table 1. In the ESTMORF-type model [*Wang et al.*, 2008; *Wang and Townend*, 2012], only the tide-averaged sediment concentration field is computed, and the advection of residual tidal flow is assumed to be negligible. The actual sediment concentration field is provided by a diffusion equation:

$$\frac{\partial(hc)}{\partial t} = w_s(c_e - c) + \frac{\partial}{\partial x}\left(Dh \frac{\partial c}{\partial x} \right) \tag{3}$$

where h is the water depth during high water of a tidal cycle to make sure that most of the considered elements is wet during the modeling (m); t is the time (s); x is the cross-flat coordinate (m), which starts at the landward boundary toward the seaward boundary (i.e., element number *1* to element number k in Figure 2); c is the sediment concentration by volume (m^3/m^3), which can be converted to sediment mass concentration (kg/m^3) by multiplying the sediment mass density ρ_s; c in (m^3/m^3) is solely for the model computation, whereas in the following text c is kept in (kg/m^3) to facilitate a straightforward comparison with previous studies; and w_s is the settling velocity for suspended sediment (m/s). As the ESTMORF-type models quantify morphological changes over an entire tidal cycle, a tide-averaged diffusion coefficient (D [m^2/s]) is used to represent the horizontal mixing process of tidal currents and waves in a tidal cycle [e.g., *Wang et al.*, 2008; *Wang and Townend*, 2012]. There is no directly corresponding parameter of D in the process-based model, and diffusion process within a tidal cycle is not explicitly considered in ESTMORF-type models [*Wang et al.*, 2008]. Other parameters in equation (3) are defined in Table 1. The boundary conditions of sediment concentration, which we used to solve equation (3), are detailed in section 2.3. The submergence condition of the elements on the upper tidal flat depends on the input tidal levels and long-term morphological development. If an element is dry ($h \leq 0$) during an entire tidal cycle, h is set to be zero. Sediment concentration field was solved numerically by the concentration balance (equation (3)).

After each tidal cycle, morphological change can be determined by the difference between c and c_e (Figure 2b):

$$\frac{\partial z}{\partial t} = \frac{1}{1-p} w_s(c - c_e) \tag{4}$$

where z is the bed level, $\partial z/\partial t$ is positive during sedimentation and negative during erosion, and p is the bed porosity. The parameters used in the DET-ESTMORF including n and D are similar to those used in the original

ESTMORF model [e.g., *Wang et al.*, 2008; *Wang and Townend*, 2012]. These parameters define the morphological time scales in the model. Detailed discussion on how to determine these parameters is given in *Wang et al.* [2008].

The numerical approach used to solve equations (3) and (4) is detailed as following: We use the common "quasi-steadiness assumption" in morphodynamic modeling; i.e., bed level was kept constant when the sediment concentration was solved, whereas the sediment concentration field was kept unchanged when the bed-level equation is solved [*Roelvink and Reniers*, 2011]. This assumption is justified because of the large difference between the morphological time scale and the time scale for sediment concentration to adjust to changing conditions. Based on this assumption, we solve the sediment concentration equation (equation (3)) using the well-known implicit Crank-Nicolson scheme [e.g., *Briggs et al.*, 2000]. Subsequently, the bed-level equation (equation (4)) is solved straightforwardly (using an explicit scheme) when the sediment concentration field is determined.

The hydrodynamic part of the DET-ESTMORF model provides τ_{90} as an input for morphodynamic modeling. The magnitude of the cross-shore current (u_c) was derived from water volume conservation in tide quasi-static propagation [*Friedrichs and Aubrey*, 1996; *Le Hir et al.*, 2000; *D'Alpaos et al.*, 2006]. As the tide rises, the water line moves landward. Onshore flows occur on tidal flats. The volume of water (ΔV) that must pass through a vertical plane (at location x) parallel to the shore equals the total water volume increase of the area landward of location x. This increase of volume can been determined from the rise of the surface level, assuming that it remains horizontal in every tidal phase. Then, the cross-shore current (u_c) that infills this volume in a time interval Δt is

$$u_c(x,t) = \frac{\Delta V(x,t)}{\Delta t h(x,t) B} \tag{5}$$

where B is the unit alongshore width of the flat. The wave propagation processes on tidal flats were quantified using SWAN (Simulating WAves Nearshore), a spectral wave model [*Booij et al.*, 1999]. The SWAN model is chosen as it can provide accurate and relatively fast wavefield estimation, which facilitates the subsequent morphodynamic modeling. The 1-D SWAN model was forced at the seaward boundary by an incident wavefield characterized by a Joint North Sea Wave Project spectrum [*Hasselmann et al.*, 1973]. Wind-induced wave growth within the model domain was excluded. For model parameters related to wave propagation processes, default values have been used (see http://swanmodel.sourceforge.net/).

The bed shear stress induced by tidal currents is

$$\tau_{\text{cur}} = \rho f_c u_c^2 \tag{6}$$

where ρ and f_c are listed in Table 1. The bed shear stress induced by waves is quantified as [*Soulsby*, 1995]

$$\tau_{\text{wave}} = 0.5 \rho f_w u_{\text{wave}}^2 \tag{7}$$

where u_{wave} is the root-mean-square value of the maximum orbital motion near the bed (this is part of SWAN output). f_w is a friction factor estimated as

$$f_w = 1.39 \left(\frac{\xi}{k_s/30} \right)^{-0.52} \tag{8}$$

where k_s is the Nikuradse roughness length $2.5 * d_{50}$, with d_{50} being the mean surface sediment grain diameter. Parameter ξ is the particle excursion amplitude close to the bed, which can be derived from SWAN model output. The mean bed shear stress under combined waves and currents during a wave cycle is calculated as [*Soulsby*, 1995]

$$\tau_m = \tau_{\text{cur}} \left[1 + 1.2 \left(\frac{\tau_{\text{wave}}}{\tau_{\text{cur}} + \tau_{\text{wave}}} \right)^{3.2} \right] \tag{9}$$

Thus, the maximum bed shear stress during a wave cycle is calculated as [*Soulsby*, 1995]

$$\tau_{\text{max}} = \left[(\tau_m + \tau_{\text{wave}} |\cos\theta|)^2 + (\tau_{\text{wave}} |\sin\theta|)^2 \right]^{0.5} \tag{10}$$

where θ is the angle between current direction and direction of wave propagation. In our study, $\theta = 0$ as both currents and wave propagation are in cross-shore direction. To avoid potential overestimation of the bed shear stress in very shallow water, τ_{max} is quantified only when the water depth is larger than 0.1 m.
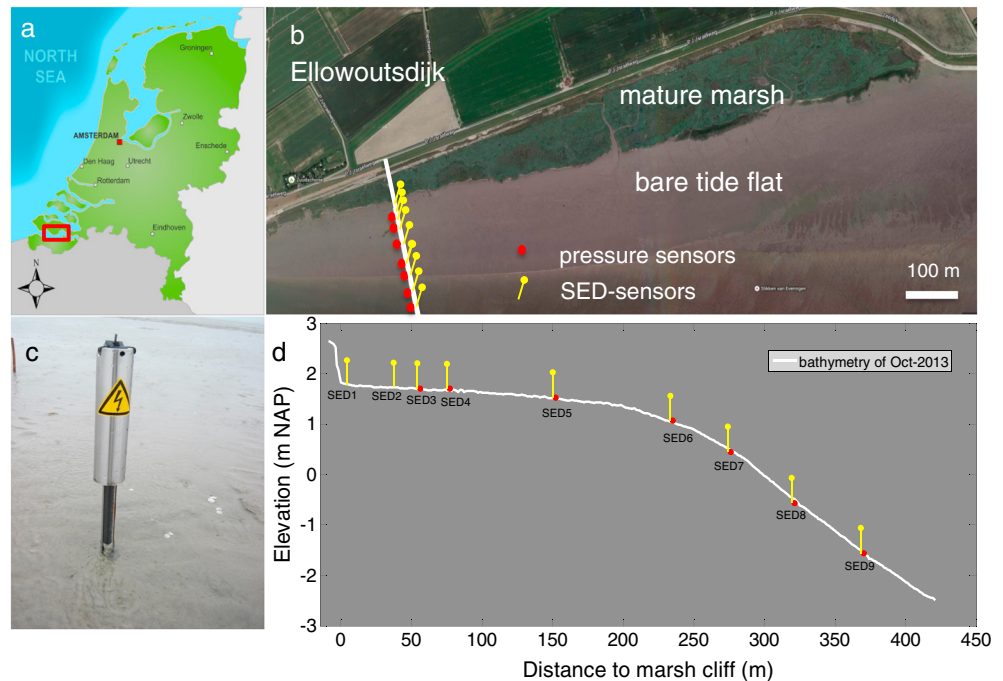
Figure 3. Location of the study site where short-term sediment dynamics and the corresponding hydrodynamics are measured. (a) The location of our study site in Westerschelde Estuary, Netherlands (the red square); (b) the deployment of the SED sensors for bed-level change measurements and the pressure sensors for wave measurements on a bare tide flat near Ellewoutsdijk in the in Westerschelde Estuar; (c) a photo of SED sensor in field; and (d) instrument deployments on the tidal flat cross section, in which $x = 0$ is the location of a cliff between the mature marsh and the bare tidal flat.

2.2. Field Measurements of Hydrodynamics and Short-Term Bed-Level Changes

To obtain field data for testing the DET-ESTMORF model performance in predicting short-term morphodynamics, we measured water levels, wave heights, and short-term bed-level changes along a tidal flat transect near Ellewoutsdijk in the Westerschelde Estuary, Netherlands (Figure 3). The Westerschelde is a mesotidal to macrotidal estuary. At the monitored tidal flat, the mean tide range is 4.1 m and it is relatively exposed to wave action induced by prevailing southwesterly winds [*Callaghan et al.*, 2010]. As the tidal flat is about 25 km upstream of the open coast, the waves are mostly locally generated by prevailing southwesterly winds.

Surface sediment samples across the tidal flat were taken monthly from January 2014 to January 2015. The yearly averaged d_{50} and d_{10} are 72 μm and 22 μm, respectively. Based on the d_{50}, τ_{cr} is estimated to be 0.10 Pa, following *van Rijn* [2007a]. The cohesive particle-particle interaction effects (including clay coating, packing, and biological effects) on τ_{cr} are not considered, as the information on clay proportion (grain size < 8 μm) was not extracted from the sediment samples. The field measurement of short-term bed-level changes was carried out almost continuously from 11 October 2013 to 16 July 2014. In this period, there were six field campaigns and each lasted 1 or 2 months. Between two campaigns, there were gaps of a few days in between, when data were being retrieved from the field.

2.2.1. Water Level and Wave Measurements

The water level and wave characteristics were measured by seven pressure sensors (OSSI-010-003C; Ocean Sensor Systems, Inc.). They are placed 0.05 m above the seabed. The measuring frequency is 5 Hz, and the measuring interval is 15 min. The measuring period in an interval is 7 min, yielding 2100 data points. The mean water depth that occurs during an interval is determined as the averaged water depth recorded in these data points. Wave conditions were reconstructed from measured pressure fluctuations, and the attenuation of the pressure signals with water depth was corrected following *Tucker and Pitt* [2001]. Bulk wave parameters, e.g., significant wave height (H_s) and peak wave period (T_p), were derived from the reconstruction.

2.2.2. Bed-Level Change Measurement

To provide data of short-term bed-level changes, we deployed automatic SED sensors (Surface Elevation Dynamic sensors) along the studied tidal flat transect (Figures 3c and 3d). The SED sensor is a novel instrument developed at Royal Netherlands Institute for Sea Research [*Hu et al.*, 2015]. When in use, it is inserted vertically into sediment bed. The electrical output of an array of 200 photovoltaic cells is used to determine the level up to which the array is covered by sediment. The distance between two cells is 2 mm, which is equal to the resolution at which bed levels and changes therein can be monitored. The length that the sensor is covered by sediment is noted as L_i, where the subscript "i" indicates the number of tide with effective measurement. The cumulative bed-level change is then the difference between L_i and the initial belowground length (L_0). The day-to-day bed-level change is then the difference between L_i and the previous effective measurement L_{i-1}. Erosion is assigned as negative values, and sedimentation is assigned as positive values.

The SED sensor does not work during nighttime or in turbid water due to the low light intensity. So the measuring window for the sensor is the emerged period during daytime. The lag between two consecutive measurements can be more than one tidal cycle. For most cases, there was at least one measurement per day from each sensor (approximately daily resolution) [*Hu et al.*, 2015]. Additionally, the transect bathymetry has been measured using a manual Differential Global Positioning System (DGPS) leveling procedure at the beginning of the survey. This DGPS measurement has been used to facilitate model domain construction.

2.3. Model Parameter Setting and Evaluations

To test the dynamic equilibrium theory embedded in the DET-ESTMORF model and to demonstrate that this model can be applied for morphological prediction, both long-term and short-term morphodynamic modeling are conducted using this model. The long-term modeling was compared qualitatively with the previous process-based modeling results, whereas the short-term modeling was evaluated quantitatively with the SED sensor measurements.

2.3.1. Long-Term Morphological Modeling

For the long-term morphological modeling, the initial tidal flat is linear for simplicity sake. The model domain extends 10 km in cross-shore direction, and the grid size is 200 m. Water-level fluctuations are schematized as

$$\zeta(t) = \frac{R}{2}\cos\left(\frac{2\pi}{T}t\right) \tag{11}$$

where R and T are the tidal range and period, respectively. T was set as 12 h, and R was varied from 2 m to 8 m to explore its effect on tidal flat morphology. The incident significant wave height at the seaward boundary (H_{s_sea}) was varied from 0.2 m to 0.8 m to test the effect of wave forcing on tidal flat morphology. In each tidal cycle, the τ_{90} is quantified every 1 h for the long-term modeling.

In order to compare DET-ESTMORF model with the previous process-based models, the parameters used for the long-term modeling are set following existing studies (Table 1). In particular, following original ESTMORF model applications [*Wang et al.*, 2008], a relation related to the tide-averaged diffusion coefficient D exists:

$$D \propto \frac{u_s^2 h_s}{w_s} \tag{12}$$

in which u_s and h_s are the scales of mixing velocity and water depth, respectively [*Wang et al.*, 2008]. In general, a diffusion coefficient is considered as the product of a velocity scale (u_s) and a length scale ($u_s h_s / w_s$) of the mixing process. In ESTMORF models with pure tidal forcing [*Wang et al.*, 2008; *Wang and Townend*, 2012], the mixing agent is tidal currents. It is then obvious to use the spatial-mean tidal current velocity as the velocity scale. As for the length scale, it is chosen as the adaptation length for sediment concentration, which is proportional to the distance a sediment particle travels in the time it needs to settle from the water surface to the bottom, i.e., $u_s h_s / w_s$ [*Wang et al.*, 2008; *Galappatti and Vreugdenhil*, 1985].

In our long-term modeling with combined tidal and wave forcing, both tidal current and wave are responsible for sediment mixing. The velocity scale (u_s) is ~0.7 m/s when the tidal range is 4 m and the incident wave height is 0.4 m. This velocity scale is based on the sum of the spatial-mean 90th tidal current velocity and wave orbital velocity on the initial linear tidal flat. The spatial-averaged water depth (h_s) is ~5 m during the high water level. w_s is chosen to be 0.0005 m/s following previous studies [*Roberts et al.*, 2000; *Liu et al.*, 2011]. To derive a reference value of D in the long-term modeling, we used equation (12) and the parameter settings of an original

ESTMORF model [*Wang et al.*, 2008]. In the original ESTMORF model, the mixing velocity scale (u_s), water depth scale (h_s), and w_s is 1 m/s, 10 m, and 0.001 m/s, respectively. $D = 1250$ m^2/s was applied in this previous model [*Wang et al.*, 2008]. In our long-term modeling, D is estimated to be 600 m^2/s based on equation (12), assuming that a constant ratio between D and $u_s h_s / w_s$ exists in the previous and the current model. This assumption seems crude, but as we are only interested in comparing the qualitative morphological behavior in the long-term modeling, the exact value of D is not very important, as long as its order of magnitude is correct.

For the long-term modeling, c_E was varied from 0.05 kg/m^3 to 0.3 kg/m^3 to test its influences on the tidal flat morphology. Correspondingly, τ_E varied in the range between 0.225 Pa and 0.6 Pa (equation (1)). At the seaward boundary of the model domain, the sediment concentration (c_k) is set to be c_E (Figure 2). This range of c_k and c_E is similar to previous process-based morphological models [*Pritchard et al.*, 2002; *Liu et al.*, 2011]. At the landward boundary, the sediment transport flux was set to be zero; i.e., the sediment concentration at the landward boundary (c_1) was equal to the concentration in the element next to it ($c_1 = c_2$).

2.3.2. Short-Term Morphological Modeling

For the short-term morphodynamic modeling, a domain was built based on the bathymetry measured at the field measurement site, which was 371 m long in the cross-shore direction with 1 m resolution (Figure 3d). The modeling elevation range is from approximately -1.70 m NAP to approximately 1.8 m NAP, at the toe of the marsh cliff. The water level and the incident wave boundary condition used for morphological modeling were provided by most seaward pressure sensor near SED9. Combined force from wave and cross-shore tidal currents is taken in to account, and it was quantified with a 15 min interval, which is the same interval for the wave measurement.

The short-term morphological modeling shared the same parameter settings as the long-term modeling listed in Table 1 with a few modifications to the in situ condition. One modification is that the setting velocity of the suspended sediment (w_s) is determined based on the following equation [*van Rijn*, 1993]:

$$w_s = \frac{(s-1)gd_s^2}{18v} \tag{13}$$

where s is the ratio between sediment density to water density, equals to 2.65; v is the kinematic viscosity coefficient (Table 1); and d_s is the suspended sediment grain size, which can be estimated based on bed sediment size measurement (d_{50} and d_{10}) as [*van Rijn*, 2007b]

$$d_s = \left[1 + 0.0006\left(\frac{d_{50}}{d_{10}} - 1\right)(\psi - 550)\right]d_{50} \tag{14}$$

where the mobility parameter is $\psi = (u_{cw}^2)/[(s-1)gd_{50}]$ with $u_{cw}^2 = u_c^2 + u_w^2$. It is noted that equation (13) is only applicable when $\psi < 550$ and $d_{50} > 62$ µm [*van Rijn*, 2007b]. As the modeled spatial-temporal mean 90th u_c and u_w is 0.06 m/s and 0.16 m/s, respectively, ψ is estimated to be 25. The mean d_{50} at the study site is 72 µm. As a result, d_s is estimated to be 20 µm and the setting velocity w_s is estimated to be 0.00036 m/s.

Another modification in the short-term modeling is that D should be adjusted to the reduced mixing velocity and water depth scales. In the short-term modeling, a water depth scale (h_s) is determined as the spatial-mean high water during high water level, i.e., $h_s = \sim2.2$ m. A representative velocity scale (u_s) can be provided by the sum of the spatial-temporal mean 90th u_c and u_w, which is 0.22 m/s. Hence, D is estimated to be 35 m^2/s based on equation (12) and the parameter settings in the previous Westerschelde model [*Wang et al.*, 2008]. However, the actual setting of D is subjected to calibration.

For short-term modeling, the sediment concentration at the seaward boundary (c_k) is determined based on suspended sediment concentration measurement at a nearby regular monitoring location (Terneuzen), which is located at the other side of the estuary, opposing to our study site Ellowoutsdijk. At Terneuzen, water samples were taken on a monthly basis by a ship operated by Dutch Department of Public Works and Water Management (Rijkswaterstaat). This survey stops during storms, and the corresponding sediment concentration is not known [*van Kessel et al.*, 2011]. The mean sediment concentration (c_{mean}) is 0.058 kg/m^3 from January 2010 to March 2014, and this measurement stopped after March 2014. As c_{mean} is a representative mean value that overlaps a part of the modeling period (October 2013 to July 2014), we assume that the overall equilibrium concentration (c_E) and the sediment concentration at the seaward boundary (c_k) equal to c_{mean} for the modeling period. Correspondingly, the uniform bed shear stress (τ_E) related to the conceptual

equilibrium is estimated to be 0.14 Pa based on $c_E = c_{mean}$ and equation (1). The τ_E is kept constant for the entire modeling period (423 tidal cycles).

The landward boundary of the short-term model is located at the cliff between the salt marsh and the bare tidal flat (near SED1 in Figure 3). Unlike the long-term model, the sediment transport flux cannot be set as zero at this boundary, as sediment can be transported from the bare tidal flat onto the salt marsh (out of the model domain) during high tide. Because of the reduced hydrodynamic forcing, the sediment concentration at this boundary (c_1) is expected to be reduced compared to that at the seaward boundary. Hence, we assumed that at this boundary $c_1 = \alpha c_k$, where α is a calibration parameter to account for the reduced sediment concentration at the landward direction ($\alpha < 1$).

The high-frequency bed-level measurement data in the periods 11 October 2013 to 11 November 2013, 17 January 2014 to 04 March 2014, and 03 April 2014 to 06 May 2014 have been used for model calibration, whereas the data in the period 20 November 2013 to 15 January 2014, 06 March 2014 to 31 March 2014, and 08 May 2014 to 12 June 2014 have been used for model validation. Prior to the morphological model evaluation, we first validated the wave modeling by comparing the modeled and measured significant wave heights (H_s) on the tidal flat transect.

All the modeling outputs (including hydrodynamic model validation, morphodynamic model calibration, and validation) are evaluated by the root-mean-square deviation (RMSD), normalized root-mean-square deviation (NRMSD), and relative bias scores (*Rel.bias*).

$$\text{RMSD} = \sqrt{\frac{\sum(\Psi_{model} - \Psi_{obs})^2}{N}} \tag{15}$$

$$\text{NRMSD} = \frac{\text{RMSD}}{|\Psi_{obs_{max}} - \Psi_{obs_{min}}|} \times 100\% \tag{16}$$

$$Rel.bias = \frac{\sum(\Psi_{model} - \Psi_{obs})}{\left|\sum(\Psi_{obs})\right|} \tag{17}$$

where Ψ_{obs} is the data from the observations and Ψ_{model} is the corresponding modeling quantify, Ψ_{obs_max} and Ψ_{obs_min} are the highest and lowest observations found in all the measuring stations, and N is the total number of data points. RMSD and NRMSD give an absolute and relative measure of the model correctness. The *Rel.bias* shows if there is any systematic defect in the model settings. In the morphological model, the Ψ_{obs} and Ψ_{model} are positive for sedimentation and negative for erosion. Therefore, *Rel.bias* is positive, if the model predicts more sedimentation (less erosion) than observation, whereas *Rel.bias* is negative, if the model predicts more erosion (less sedimentation) than observation.

For model calibration, we tuned D and α to obtain a minimum RMSD in cumulative bed-level changes compared to the observations. To test if the variation in D has a significant impact on the model performance, a sensitivity analysis based on RMSD and *Rel.bias* assessment was conducted. D was varied from 0.1 to 100 m²/s, while α was fixed as the calibrated value in the sensitivity analysis. Similarly, to test the model sensitivity to α, the value of α was varied from 0.05 to 0.5, while D was kept constant as the calibrated value. Parameter $\alpha = 0.05$–0.5 means that the sediment concentration at the landward boundary (marsh cliff) was reduced to 5%–50% compared to that at seaward boundary.

3. Results

3.1. Long-Term Tidal Flat Morphological Evolution Modeling

To test the dynamic equilibrium concept embedded in the DET-ESTMORF model, long-term tidal flat morphodynamic modeling was carried out with various hydrodynamic and sediment availability conditions, which is compared qualitatively with previous process-based modeling studies.

3.1.1. Tidal Flat Evolution Under Contrasting Forcing

The initial linear tidal flat profile was forced by tide only or combined tide-wave forcing in the long-term modeling (Figure 4). With the contrasting forcing conditions, the morphological response of the tidal flat is very different (Figures 4c and 4f). When the tidal flat is forced only by tide, the initial profile will first adjust its shape quickly to a steeper slope (from approximately $t_0 - t_2$), and then the profile can maintain such a slope
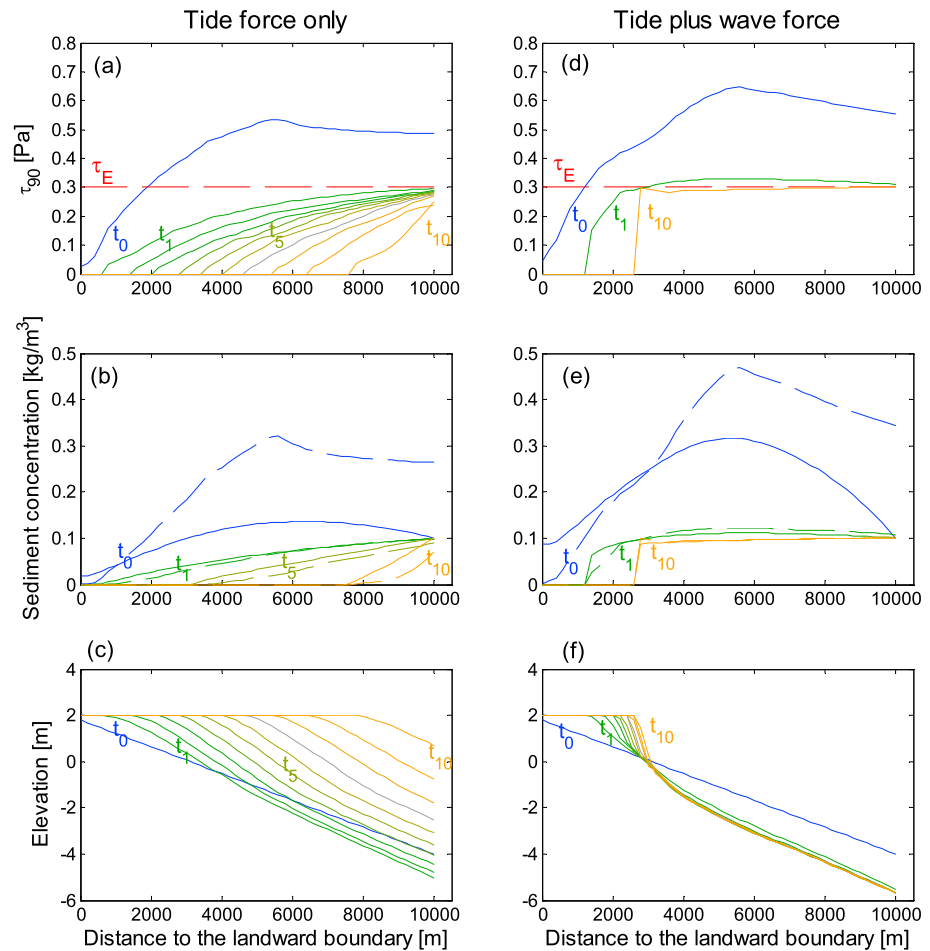
Figure 4. Long-term tidal flat evaluations under different hydrodynamic forcing. The model inputs are the overall equilibrium concentration, (c_E) is 0.1 kg/m^3, tidal range (R) is 4 m, and incident signification wave height (H_{s_sea}) is 0.4 m. In each panel, t_0, t_1, …, t_{10} indicate the time sequence of the evaluation, with t_0 being the initial conditions. Between two time steps, e.g., between t_0 and t_1 the time span is about 3,000 tidal cycles. (a and d) The distribution of 90th percentile bed shear stress (τ_{90}) on tidal flats. The red dashed line indicates that the uniform bed shear stress for equilibrium (τ_E) is 0.3 Pa, corresponding to the imposed c_E. (b and e) The distribution of the local equilibrium concentration (c_e, dashed line) and the actual concentration (c, solid line). The difference between these two determines the local bed-level changes. (c and f) The tidal flat morphological evolution. At the high-water-level mark (2 m), plateaus develop overtime as tidal flats prograde seaward.

and prograde seaward. In contrast, when wave forcing is added, the tidal flat cannot continuously prograde seaward (Figure 4f). After an initial quick adjustment of the profile slope (from $t_0 - t_1$), the profile seems to reach a quasi-static equilibrium around t_{10}. At this stage, the difference between two consecutive profiles is almost negligible. Notably, at t_{10}, the distribution of τ_{90} in combined wave and tide condition is almost uniform and equals to τ_E over the entire tidal flat (Figure 4d), which is different for the condition with only tide force and will be discussed in the following section.

A "plateau" develops at the high water mark (elevation = 2 m) as the model only deals with the domain below the high water level. Below the plateau, the tidal flat under pure tidal forcing generally has a convex shape. The tidal flats under combined tide and wave forcing have a distinctive concave shape. Additionally, initial profile slope has no effect on the general evolution process or the stable profile bathymetry but only influences the time span to reach a stable slope (data not shown).

The predicted contrasting profile evolution trajectories can be explained by the embedded dynamic equilibrium theory in the model. For the initial condition with pure tide forcing (t_0 in Figure 4a), τ_{90} is uniform and higher than the τ_E (0.3 Pa) on the lower part of the profile. On the upper tidal flat, it decreases gradually toward landward direction as the (tide-driven) passing water volume is reduced (ΔV in equation (5)). A similar

distribution of τ_{90} has been shown in previous studies [*Le Hir et al.*, 2000; *Pritchard et al.*, 2002]. According to equation (2), the spatial distribution of τ_{90} has a similar distribution pattern of the local equilibrium concentration c_e (t_0 in Figure 4b). It shows that the lower tidal flat has the tendency of erosion (i.e., high c_e) and the upper tidal flat has the tendency of sedimentation (i.e., low c_e). The actual sediment concentration has a unimodal shape (c at t_0 in Figure 4b), which is derived by the sediment transport function (equation (3)). The lower c at the upper and lower flats is induced by the subscribed boundary conditions. A high c at the middle flat is likely caused by sediment erosion over the lower part of the flat bed. Finally, the difference between c and c_e determines the bed-level changes (equation (4)): the deficits of c compared to c_e on the lower tidal flat lead to erosion, whereas the surplus of c on the upper tidal flat leads to sedimentation (see t_0 in Figures 4b and 4c). Thus, the whole flat at t_1 becomes steeper than the original profile at t_0.

After the initial stage (since t_1 onward), a positive feedback mechanism seems to govern the tidal flat development under pure tidal forcing. At t_1, τ_{90} drops below τ_E over the entire tidal flat because the tidal current velocity is reduced on the steeper tidal flat (i.e., increasing h in equation (5)). Hence, the entire tidal flat has the tendency of sedimentation, which is also indicated by the low c_e over the tidal flat (see t_1 in Figure 4b). The derived actual sediment concentration field at t_1 is higher than the c_e in the area approximately $x < 4000$ m, which leads to sedimentation on the upper part of the tidal flat. The infilling of the upper profile further reduced the overall cross-shore current velocity because of the reduction of ΔV in equation (5). It means that the τ_{90} over the whole tidal flat will be further reduced (Figure 4a). Thus, the sedimentation on the profile continues and the positive loop is formed, which results in the seaward progressing profile ($t_1 - t_0$ in Figure 4c).

For the case with cooccurring wave forcing, the positive feedback does not occur and the tidal flat eventually approaches to a quasi-static equilibrium (Figure 4f). At t_0, τ_{90} is higher than that in a pure tide condition due to the addition wave force (Figure 4d), but the overall distribution pattern of τ_{90}, c_e, and c is similar. As the profile moves seaward ($t_1 - t_0$ in Figure 4f), the wave forcing becomes more competent in the shallow (upper) tidal flat to compensate the attenuated tidal current force (Figure 4d). At t_{10}, the τ_{90} becomes almost uniform and equals to the τ_E on the tidal flat. Correspondingly, the driver for morphological changes vanishes; i.e., the difference between c and c_e approaches to zero (t_{10} in Figure 4e). In such a condition, the tidal flat reaches a relatively stable equilibrium state (t_{10} in Figure 4f).

3.1.2. Tidal Flat Profile in Various Conditions

In order to test the long-term modeling performance comprehensively, we use the DET-ESTMORF model to predict tidal profile shape under various forcing and sediment supply conditions (Figure 5). In the previous section, it has been shown that a tidal flat under pure tidal forcing can continuously progress seaward with a constant slope (Figure 4c). A static equilibrium state is not possible in such a condition. Considering this, we compared profile shapes in different conditions when all of them have achieved stable slopes (e.g., t_5 in Figure 4c). The modeling outcomes can be compared qualitatively with previous studies.

It is clear that a tidal flat profile becomes steeper with an increase of tidal range (Figure 5a). The increase in steepness can be explained by the insights gained from Figures 4a and 4c. The larger tidal range will lead to larger passing volume (ΔV) in equation (5), which means a higher current velocity and a higher τ on the lower tidal flat. Then, stronger erosion can occur on the lower flat to make the whole profile steeper compared to the cases with smaller tidal ranges. For the cases with larger tidal range, the same initial profile takes longer to reach a stable slope, as there is more sediment to be eroded at the beginning of the simulation.

The width of the tidal flat, i.e., the distance from high water to low water, increases as the tidal flats prograde seaward. As the profiles with larger tidal ranges take more time to reach stable slopes, they have smaller width within the same time span. However, the width difference may be not important as all the profile width increases over time in this condition and the actual width may depend on the considered time scale.

The modeling results also show that if the sediment supply is increased in the system, tidal flat width increases and profile steepness reduces accordingly (Figure 5b). Furthermore, a rise in H_{s_sea} leads to more concave profiles with smaller profiles width (Figure 5c). It is worth noticing that under combined tide and wave forcing, the lateral position of the relative stable equilibrium profile may depend on the relative strength of wave forcing compared to the tidal forcing. If wave forcing is stronger than tidal forcing (high H_{s_sea} conditions), tidal flats can reach a relative stable equilibrium profile in a shorter time span and can stay
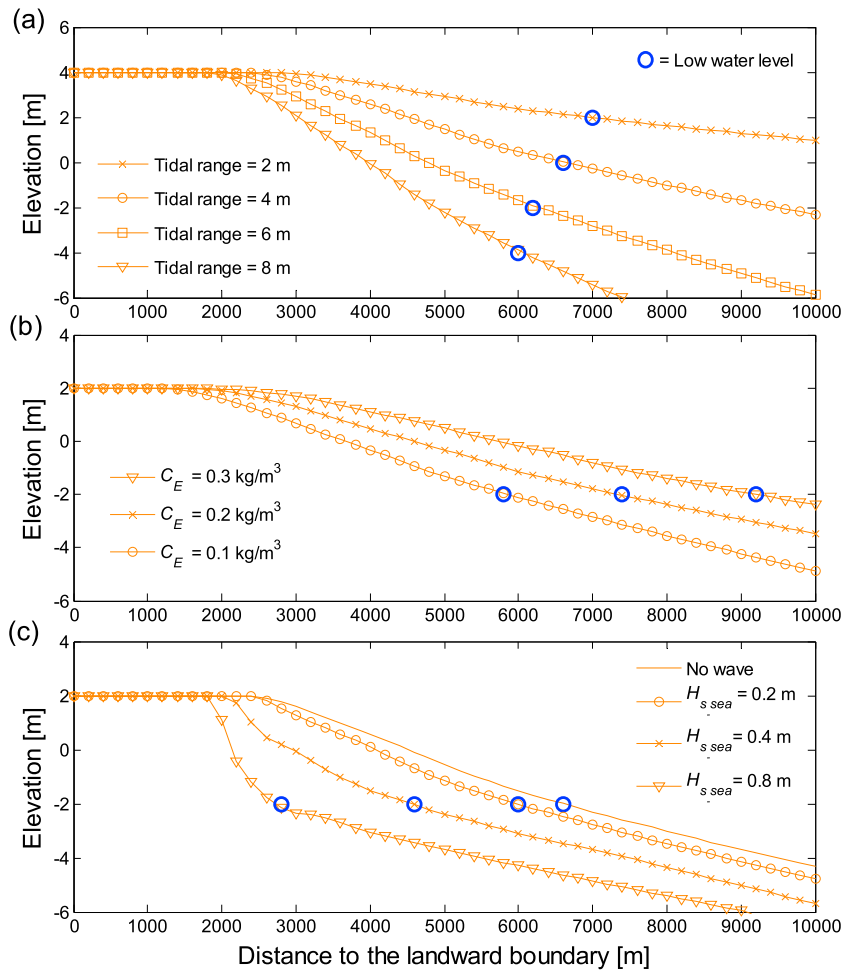
Figure 5. Predicted tidal flat profiles with different conditions. (a) Tide only condition, the overall equilibrium concentration (c_E) is 0.1 kg/m^3; correspondingly, the uniform bed shear stress for equilibrium (τ_E) is 0.3 Pa. The tidal range (R) varies from 2 to 8 m. The four profiles are moved vertically to make the high-water-level coincident. The shown profiles are after 10000 tidal cycles, when relative constant profile slopes have been reached. (b) Tide only condition, R is 4 m. C_E is 0.1, 0.2, and 0.3 kg/m^3; accordingly, τ_E is 0.3, 0.45, and 0.6 Pa. The shown profiles are after 5000 tidal cycles, when relative constant profile slopes have been reached. (c) Tide plus wave, R is 4 m; C_E is 0.1 kg/m^3; τ_E is 0.3 Pa; and wave height from the seaward boundary (H_{s_sea}) is 0, 0.2, 0.4, and 0.8 m. The shown profiles are after 10000 tidal cycles, when the profile with 0.8 m incident wave has reached a quasi-stable equilibrium and other profiles are still migrating seaward.

closer to the landward boundary. For the case with weaker wave forcing (low H_{s_sea} conditions), the profile will keep migrating seaward until the wave forcing becomes significant in the shallow areas to enable a uniform distribution of τ_{90}. For instance, the profile with 0.8 m H_{s_sea} approaches to a stable equilibrium after about 10,000 tidal cycles (Figure 5c), whereas other profiles with 0.4 m H_{s_sea} will keep propagating seaward after the same time span and will reach a stable equilibrium after about 30,000 tidal cycles (see t_{10} in Figure 4f).

3.2. Short-Term Bed-Level Dynamic Modeling

To test the DET-ESTMORF model in a quantitative way, we compared the modeling results with the hydrodynamic and morphodynamic measurements at the study site in the Westerschelde Estuary. This modeling exercise also demonstrates how this dynamic equilibrium theory can be applied for realistic morphological predictions.

3.2.1. Hydrodynamic Modeling at the Study Site

First, we evaluated the wave modeling by comparing the modeled significant wave height against the measurement along the monitoring transect (Figure 3). The comparison is based on one of the monitoring period
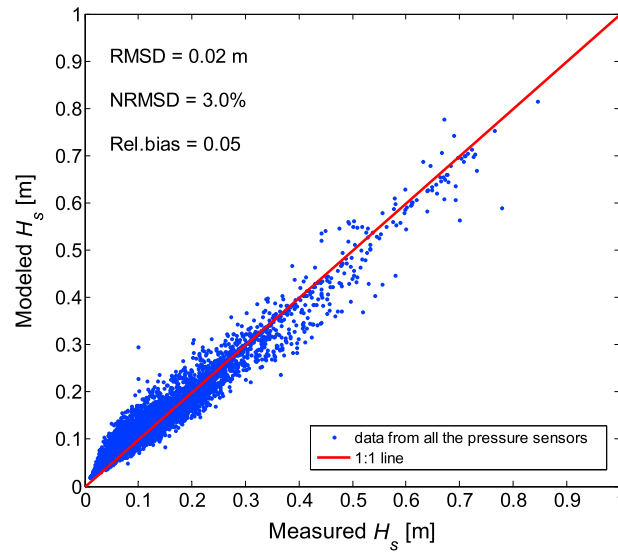
Figure 6. Comparison of modeled and measured significant wave height (H_s) on the studied tidal flat. The wave measurements are obtained by an array of press sensors shown in Figure 3. The shown data are from the measuring period 11 October 2013 to 11 November 2013, and the measuring interval is 15 min. The total number of data points is 6418 in this period, which includes a severe storm event with maximum significant wave height being 0.8 m on this relatively shallow tidal flat.

(11 October 2013 to 11 November 2013). During this period, the RMSD and NRMSD are 0.02 m and 3.0%, respectively (Figure 6). Additionally, the *Rel.bias* is 0.05, which is close to zero (i.e., no bias). Hence, the comparison shows that the predicted H_s agrees well with the wave measurement, indicating the reliability of using the SWAN model for wave simulations at the study site.

For the short-term morphology modeling, bed shear stress is quantified every 15 min to count for the changing hydrodynamic forcing conditions. Within a tidal cycle, the bed shear stress distribution varies with the tidal phase and the incident wave conditions (Figure 7). For each time step shown in Figure 7, the bed shear stress distribution generally has a unimodal shape, which is likely induced by wave breaking in shallow areas. The shown tidal cycle has a mean incident H_s equals to 0.26 m, with the maximum and minimum being 0.08 m and 0.43 m, respectively. The location of the peak bed shear stress moves laterally on the tidal flat with the changing tidal phase. Based on the bed shear stress time series at each location, the τ_{90} is derived as an input for the morphological prediction following *Friedrichs and Wright* [2004] and *Friedrichs* [2011].
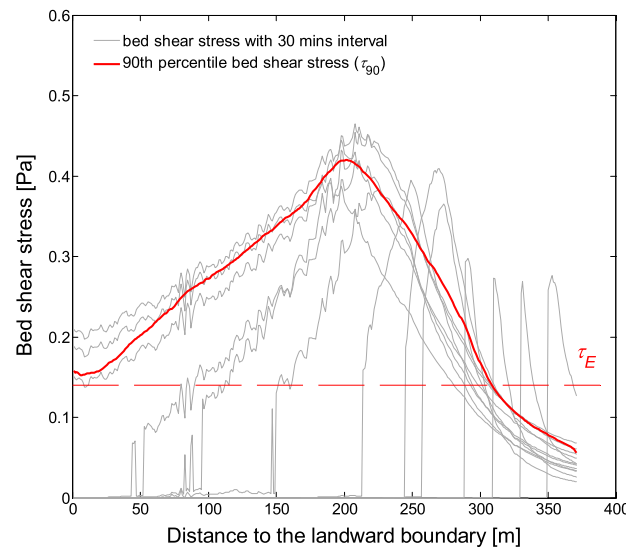

Figure 7. A demonstration of bed shear stress in a tidal cycle and the corresponding 90th percentile bed shear stress (τ_{90}) for morphodynamic modeling at the study site; the estimated uniform bed shear stress for equilibrium (τ_E) is 0.14 Pa, which is plotted as the horizontal dashed line. In this tidal cycle, the incident significant wave height (H_{s_sea}) varies from 0.08 m to 0.43 m, with the tide-averaged H_{s_sea} being 0.26 m; bed shear stress is quantified every 15 min in the model and plotted here every 30 min for demonstration.

3.2.2. Short-Term Bed-Level Change Modeling and Measurements

Quantitative evaluation of the morphological model is carried out by calibrating and validating the DET-ESTMORF model with the SED sensor measurements. D and α are calibrated to be 30 m^2/s and 0.1 (-), respectively, as this setting leads to the minimum RMSD (2.19 cm) in the calibration. Subsequently, these settings were applied to both calibration and validation of the morphodynamic modeling. An example of the modeled cumulative bed-level changes and the corresponding SED sensor data is shown in Figure 8. The cumulative bed-level changes give an overview of the morphological evaluation during a model validation period: 20 November 2013 to 14 January 2014. Overall, the predicted bed-level changes fit reasonably well with the observed erosion trends of most stations (Figure 8). On the upper tidal flat (i.e., stations SED1, SED3, to SED6), the model prediction agrees well with the measurements. At station SED2, however, the model does
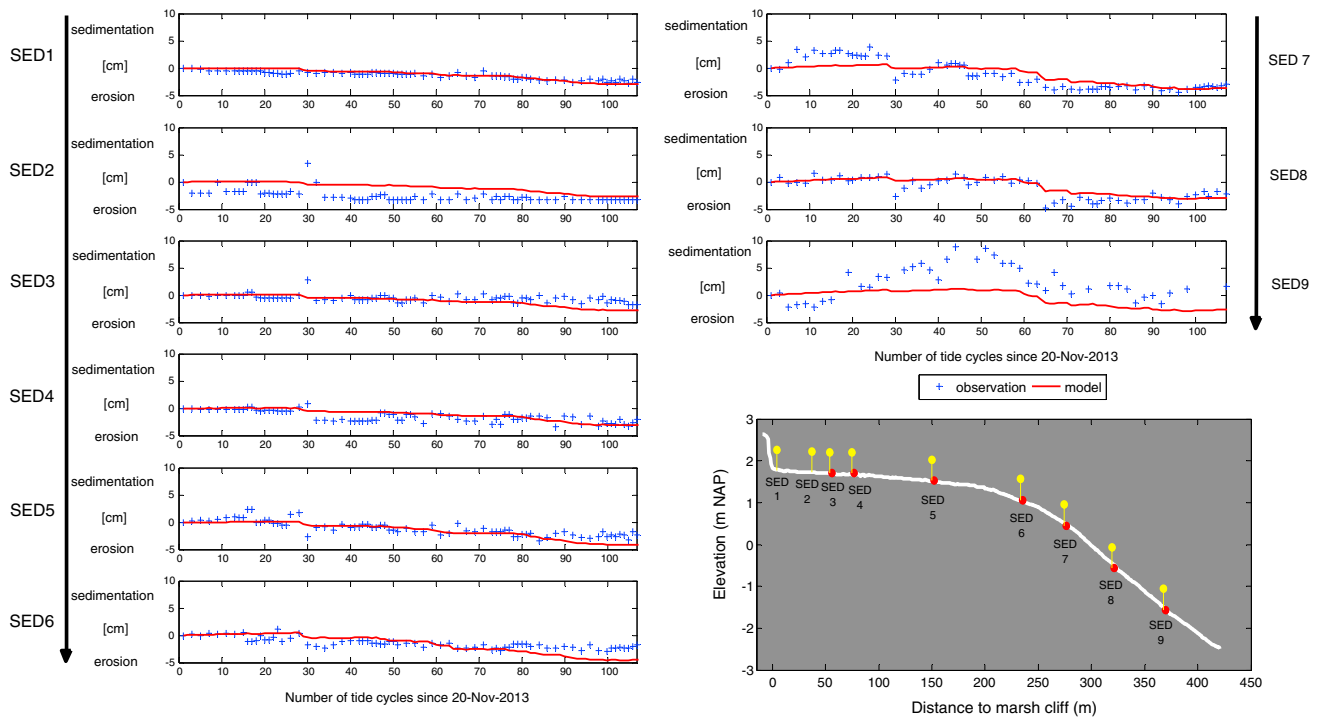
Figure 8. Modeled and measured cumulative short-term bed-level changes, which are the bed-level changes of each period compared to the initial bed level. Positive values mean sedimentation, and negative values mean erosion. The yellow symbols in the bottom right plot indicate SED sensor stations, and the red symbols indicate pressure sensors. The demonstrated data are from the period 20 November 2013 to 15 January 2014. The total number of observation points during this period is 627. Similar plots of the other five modeling periods are provided in the supporting information.

not capture the sudden bed-level change occurred during the first a few tidal cycles, and such an error retains during the following tidal cycles. At lower stations SED7 and SED8, the agreement between model prediction and measurement is still reasonably good. Specially, at these two stations, the model captures a storm event during tidal cycle 64 (tidal-averaged $H_{s\_sea} > 0.55$ m). Although the magnitude of the erosion during this storm seems underestimated, the sudden morphodynamic response is reproduced well by the model. The model cannot reproduce the high degree of morphodynamics at the most seaward station (SED9), which will be discussed in the following section.

An overview of the model calibration and validation using all the SED sensor measurements shows that the overall model performance is good (Table 2). The evaluation is conducted based on both cumulative and daily bed-level changes. For the evaluation based on cumulative bed-level changes, the mean RMSD value of the three calibration periods is 2.25 cm, whereas the mean RMSD value of the validation periods is 1.58 cm. The smaller mean RMSD value in the validation periods indicates a good predictive capability of

Table 2. Model Calibration and Validation Against the SED Sensor Measurements[a]

Bed-Level Measurement Periods	Data Usage	Total Number of Observations	RMSD (cm)	NRMSD (%)	Rel.bias (-)
11 Oct 2013 to 11 Nov 2013	calibration	292	3.00 (1.02)	36% (19%)	0.70 (0.13)
20 Nov 2013 to 15 Jan 2014	validation	627	1.49 (0.90)	10% (15%)	−0.04 (−0.04)
17 Jan 2014 to 04 Mar 2014	calibration	508	1.61 (0.91)	20% (19%)	−0.49 (−0.01)
06 Mar 2014 to 31 Mar 2014	validation	291	1.56 (1.03)	31% (22%)	0.84 (0.08)
03 Apr 2014 to 06 May 2014	calibration	280	2.13 (1.22)	27% (20%)	0.57 (−0.01)
08 May 2014 to 12 Jun 2014	validation	235	1.70 (0.91)	20% (20%)	0.08 (−0.02)

[a]The data without brackets are based on the cumulative bed-level changes, which is the difference between the current bed level and the initial bed level; the data in brackets are based on the daily bed-level changes, which is the difference between the current bed level and the bed level of the previous day(s). All the data are averaged in space over the SED sensor stations (see Figure 3).
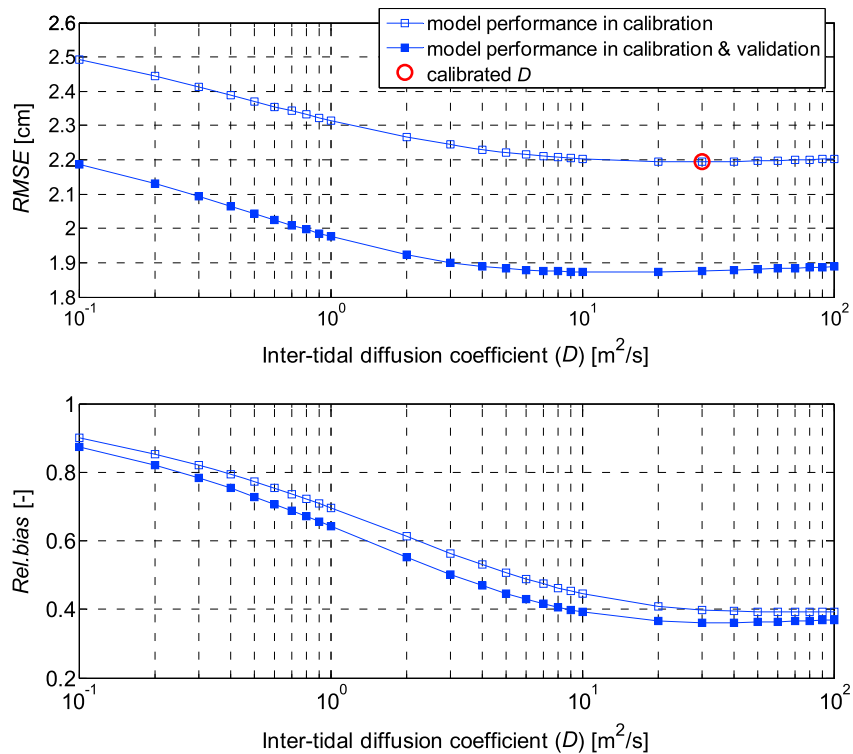
Figure 9. Sensitivity analysis of the modeling performance related to tide-averaged diffusion coefficient (D). The performance is evaluated by (top) root-mean-square deviation (RMSD) and (bottom) relative bias scores (*Rel.bias*), which are based on cumulative short-term bed-level changes. The "model performance in calibration" is based on comparing the modeled and measured data that are used for calibration (see Table 2), and the "model performance in calibration and validation" is based on the entire data set. D is calibrated as 30 m^2/s, as it leads to the least RMSD during the calibration.

the model. The mean NRMSD of the cumulative bed-level changes in calibration and validation periods is 28% and 20%, which implies that the modeling errors is relatively small compared to the observed overall morphodynamic activities.

For the evaluation based on daily bed-level changes, the RMSD and the NRMSD are generally smaller than those based on the cumulative bed-level changes. It is because this assessment is based on the changes over two consecutive measurements, and the possible influence of the errors modeled in previous periods is excluded (e.g., the second data point at SED2 in Figure 8). In this assessment, *Rel.bias* values are closer to zero compared to those with cumulative bed-level changes, which indicate a weaker bias favoring sedimentation (Table 2).

Sensitivity analysis is conducted by evaluating the model performances with varying D and α. The measured and modeled cumulative bed-level changes are compared for the sensitivity analysis. RMSD reaches minimum (i.e., 2.19 cm) during calibration when D is 30 m^2/s and α is 0.1. Thus, in the sensitivity analysis of α (0.05–0.5), D is kept constant as 30 m^2/s. All the available data (see Table 2) are used in the sensitivity analysis. As α varies in the range of 0.05 to 0.5, RMSD varies 0% to 4% compared to the RMSD with the calibrated D and α. Therefore, the variations in α do not significantly affect the model accuracy.

Similarly, in the sensitivity analysis of D (0.1–100 m^2/s), α is kept constant as 0.1. With the minimum and maximum D values, the corresponding RMSD is only 14% and less than 1% higher compared to the minimum RMSD in the test with only calibration data (Figure 9). In the test with both calibration and validation data, the RMSD values are smaller compared to that with calibration data. In this test, the minimum RMSD (1.87 cm) is reached when D is 10 m^2/s. As D increases from 0.1 to 100 m^2/s, RMSD becomes fairly constant around 1.90 cm, when D is higher than 1 m^2/s. Therefore, in the test with only calibration data and the test with all the data, the model performance is not significantly influenced by D in terms of RMSD.

It is also noted that in the test with calibration data, the *Rel.bias* drops from approximately 0.9 to 0.4 as D increases from 0.1 to 100 m^2/s. The test with both calibration and validation data shows a similar trend,

but the *Rel.bias* values are closer to zero compared to the calibration case. The *Rel.bias* reduction with the increasing D means that the degree of overestimating sedimentation (underestimating erosion) reduces. It may be caused by the fact that with larger D more wave-eroded sediment can be transported elsewhere and less sediment will stay around the original location waiting to settle onto the seabed again. When $D > 10 \, \text{m}^2/\text{s}$, the *Rel.bias* stays relatively constant at 0.4 in both tests. Thus, the model performance (in term of *Rel.bias*) is not significantly influenced when $10 \leq D \leq 100 \, \text{m}^2/\text{s}$, and the model has a constant tendency favoring sedimentation or underestimating erosion. The reason of this constant tendency is discussed in the following section.

4. Discussion

4.1. Testing Dynamic Equilibrium Theory in Long-Term Morphological Modeling

In this study, we implemented the dynamic equilibrium theory in the DET-ESTMORF model. The long-term DET-ESTMORF modeling outcome can be compared with previous process-based modeling results that were summarized in *Friedrichs* [2011]. As the process-based modeling does not rely on the dynamic equilibrium theory for morphodynamic modeling, the comparison between these two types of model is an independent and direct test of the theory. The long-term morphological predictions agree well with the previous process-based modeling, which implies the validity of the dynamic equilibrium theory.

In the long-term modeling, the model predicts the profile to attain a convex or concave shape when it is forced by pure tide or combined tide and wave actions (Figures 4 and 5), which agrees with the previous process-based models and the field observations summarized in *Friedrichs* [2011]. We also show that predicted tidal flat bathymetry varies in a similar way as the previous process-based models when tidal range, incident wave height, and offshore sediment supply are changed [*Roberts et al.*, 2000; *Pritchard et al.*, 2002; *Liu et al.*, 2011].

Furthermore, the predicted dynamic behavior of the tidal flat also agrees with the previous studies that are summarized in *Friedrichs* [2011]. For the case with only tide force, the predicted seaward migrating tidal flat (see Figure 4c) agrees with previous process-based modeling studies and observations from Jiangsu coast for instance [*Pritchard et al.*, 2002; *Waeles et al.*, 2004; *Liu et al.*, 2011]. In previous process-based models, the same profile morphological behavior was explained by nonzero tidal-averaged settling lag that favors a small but persistent net sediment import [*Pritchard et al.*, 2002]. However, it is also noted that a previous process-based model have shown stationary tidal flat equilibrium under tidal-only forcing [*Roberts et al.*, 2000]. The difference in the tidal flat morphological behavior (stationary and seaward migrating) can be explained by the different hydrodynamic models applied [*Friedrichs*, 2011].

The continuous propagating behavior in our model is induced by a positive feedback process that is governed by the dynamic equilibrium theory embedded in the DET-ESTMORF model (Figures 4a and 4b). The different explanations offered by these two different types of models may seem misleading for the morphodynamic interpretation. However, it should be noted that the dynamic equilibrium theory is meant to describe the overall tidal flat morphological behaviors rather than elaborating the detailed physical processes like the process-based models. Hence, based on this theory, the DET-ESTMORF model may offer alternative explanations for the same morphological behavior without handling the subtle intertidal sediment dynamics.

Additionally, the model prediction also shows that only when wave forcing is included, the tidal flat may reach a relative stable equilibrium profile (Figure 4f), which agrees with the previous process-based modeling studies as well [*Waeles et al.*, 2004; Maan et al., submitted]. This can be explained by the embedded dynamic equilibrium theory as the wave force is needed to compensate the damped tidal current force in the shallow areas to minimize the spatial gradients in bed shear stress and eventually achieve a relative static equilibrium. The model further shows that tidal flat concavity increases with the incident wave forcing, which is also in line with the previous modeling [*Roberts et al.*, 2000] and field studies [*Bearman et al.*, 2010; *Friedrichs*, 2011].

4.2. Testing Dynamic Equilibrium Theory in Short-Term Morphological Modeling

Morphological modeling studies often focus on a time scale of years to decades in order to project long-term tidal flat developments with possible influence of sea level rise and/or sediment supply changes [*Roberts et al.*, 2000; *Pritchard and Hogg*, 2003; *Fagherazzi et al.*, 2006, 2012; *Kirwan et al.*, 2010; *Mariotti and Fagherazzi*, 2010]. However, a long-term concurrent data set including tidal flat bathymetry, offshore

sediment concentration, and weather conditions (stormy/calm periods) is rare for quantitative model evaluation [*Pritchard and Hogg*, 2003]. In this study, we adjust the DET-ESTMORF model to quantify the short-term bed-level changes so that the high-frequency wave and SED sensor measurement can be used for quantitative model evaluation.

Moreover, the short-term morphodynamic modeling serves as a demonstration of applying the dynamic equilibrium theory for realistic applications. Recent studies have shown that predicting short-term bed-level fluctuations can be important for the understanding of vegetation establishment patterns on bare tidal flats [*Balke et al.*, 2011, 2013, 2014; *Han et al.*, 2012]. Thus, this DET-ESTMORF model can be a relevant tool for vegetation colonization prediction. In contrast, the original analytical model [*Friedrichs and Aubrey*, 1996] can only provide the idealized profile bathymetry when a static equilibrium has been achieved. Such a model is helpful in understanding the typical large-scale tidal flat behaviors but may be less useful for realistic morphological predictions. Overall, the model prediction fits reasonably well with the bed-level measurement regarding to the RMSD and NRMSD evaluations (Table 2). During some storm events, the prediction clearly follows the sudden daily changes (stations SED7 and SED8 in Figure 8). The results imply that the dynamic equilibrium theory can be trustworthy and useful in explaining the morphodynamics in a daily to monthly time scale. The DET-ESTMORF model can provide reasonable prediction accuracy despite its simple structure.

The ESTMORF-type models quantify the morphological changes over an entire tidal cycle, so that the tide-averaged diffusion coefficient (D) is employed to account for the overall sediment mixing due to both tidal and wave motion in a tidal cycle. The D used in the short-term modeling is calibrated to be $30\,m^2/s$, and it is estimated to be $35\,m^2/s$ following equation (12). The two values are fairly close, suggesting the usefulness of the parameter setting guidelines in *Wang et al.* [2008]. The sensitivity analysis further shows that the model performance is not sufficiently influenced by the variations of D and α. However, it is also noted that the predictions show a bias toward sedimentation (Figure 9). It may be caused by the fact that some of the erosion events cannot be represented accurately in the model, and these errors remain in the following analysis of the cumulative bed-level changes (e.g., SED2 in Figure 8). It is also noticed that the short-term morphological changes at the deepest SED sensor station cannot be reproduced very well (i.e., SED9 in Figure 8). It may be because alongshore currents play an important role in this relatively deep area, which is not accounted for in our 1-D model.

4.3. Defining Uniform Bed Shear Stress τ_E

Defining τ_E is of fundamental importance in the dynamic equilibrium theory as it describes the tidal flat equilibrium state. The dynamic equilibrium of a tidal flat is associated with its local hydrodynamic forcing, sediment supply, and other factors [*Friedrichs*, 2011]. Similarly, the long-term averaged suspended sediment concentration on the tidal flat is also affected by these factors. Hence, we define τ_E as the bed shear stress that can maintain a constant overall equilibrium concentration (c_E) in water column (equation (1)). Effectively, τ_E depends on c_E in the DET-ESTMORF model.

We find that this definition of τ_E fits well with the dynamic equilibrium theory and previous findings: (1) the dependency of τ_E on c_E has also been suggested by previous process-based modeling. For instance, *Pritchard et al.* [2002] and *Liu et al.* [2011] have shown that on the tidal flats with higher sediment input (i.e., higher c_E), τ_E is larger when a constant profile slope has been reached. Hence, in process-based models, τ_E on the eventual tidal flats may be determined by c_E via long-term morphodynamic feedback; (2) in realistic case studies (reference herein), c_E can be determined as the long-term background sediment concentration in the study areas, which generally accounts for the combined effect of the local forcing and sediment supply conditions. If the sediment supply in an area is increased by natural or anthropogenic processes (higher c_E), τ_E will increase accordingly, i.e., move τ_E to a higher level in Figure 2a. Thus, the entire system would shift toward the direction favoring deposition. In contrast, if the sediment supply reduces, the whole system will become favoring erosion instead. Similar tidal flat morphological response has been reported in previous studies [*Friedrichs*, 2011].

4.4. Strengths and Limitations of the DET-ESTMORF Model

Judging from the modeling philosophy, the DET-ESTMORF model clearly adapts a top-down approach [*Stive and Wang*, 2003; *Roelvink and Reniers*, 2011]. That is, the model starts with describing the salient feature of tidal flat morphology then move downward to attend more detailed aspects such as hydrodynamics and sediment conservation. The process-based models (e.g., Delft3D), on the other hand, generally adapt a

bottom-up approach. They start with a meticulous elaboration of the relevant physical processes and then reveal the morphological features.

For all models, the critical question is about understanding and depicting the governing processes. Depending on the nature of the processes and the purposed theory, we may choose a suitable modeling approach to implement such an understanding. In many cases, process-based models are powerful tools to provide insights and predictions of tidal flat morphology [*Lesser et al.*, 2004]. Yet for the primary purpose of the present study, i.e., directly testing the dynamic equilibrium theory, they may have difficulty in satisfying the underlying assumption of the theory, as a uniform bed shear stress distribution rarely exists.

The main strengths of the DET-ESTMORF model can be summarized as (1) the need of a prescribed equilibrium state in this model gives us a handle to implement and directly test the dynamic equilibrium theory by evaluating the model performance; (2) compared to the original analytical solution [*Friedrichs and Aubrey*, 1996] that only deals with the idealized condition with uniform force, the DET-ESTMORF model applies the dynamic equilibrium theory in realistic morphological predictions with spatially and temporally varying bed shear stress, which largely broadens the model application range; (3) for long-term morphological modeling, DET-ESTMORF prediction can always converge to a morphological equilibrium close to reality because of the underlying dynamic equilibrium theory. In process-based models, however, minor errors over each tidal cycle may accumulate over time and lead to unrealistic predictions in long-term [*Wang et al.*, 1998, 2008]; (4) for short-term morphodynamic modeling, the DET-ESTMORF model provides a simple but sufficient tool to predict frequent tidal flat bed-level changes that affect critical ecological processes such as vegetation establishment.

In order to test dynamic equilibrium theory, the DET-ESTMORF model only involves the necessary processes for morphological simulations. However, the simple configuration of the model also leads to some limitations. First, one of the main limitations is that alongshore currents were not considered in the current 1-D model, which can be important for the tidal flat morphodynamic activities at the lower elevations (e.g., station SED9 in Figure 8) [*Gong et al.*, 2012]. Second, it is noted that detailed erosion processes related to wave breaking are not explicitly accounted for in the model. The wave breaking effect is considered in a bulk way by using the breaking-induced high bed shear stress in morphological modeling. Third, detailed hydrodynamic processes including friction variations, momentum advection, and ebb-flood asymmetry are not included in the current simple tidal current model. For the sake of simplicity, we neglect the possible influence of multiple sediment fractions and potential biogeomorphological interactions on tidal flat morphology. Finally, model calibration is always needed when applying this model to a new area, since parameters like tide-averaged diffusion coefficient D cannot be derived from measurements directly [*Wang et al.*, 2008]. To further improve the morphological prediction, more physical processes can be included, such as alongshore currents, friction variations, momentum advection, sediment mixing as well as biostabilization/bioturbation.

5. Conclusion

In this study, we combined the dynamic equilibrium theory and the hybrid (ESTMORF) modeling approach to create the new DET-ESTMORF model. Applying this model, we showed that the dynamic equilibrium theory could be applied for both long-term and short-term morphodynamic predictions with spatiotemporally varying bed shear stress. The long-term modeling not only derives the classic convex or concave profile shapes with corresponding force conditions but also presents similar dynamic behavior as that found in previous process-based modeling studies. Furthermore, the short-term bed-level change modeling also showed a reasonable good agreement with the field measurements. The good model performance in both long-term and short-term modeling tests indicates that the embedded dynamic equilibrium theory is valid and the model itself is useful in morphological predictions. It is noted that the current DET-ESTMORF model only considers a limited number of physical processes, which may cause prediction errors. However, the simple model structure may provide an open platform to incorporate additional biotic and abiotic processes for tidal flat landscape evolution studies.

References

Amoudry, L. O., and A. J. Souza (2011), Deterministic coastal morphological and sediment transport modeling: A review and discussion, *Rev. Geophys.*, 49, RG2002, doi:10.1029/2010RG000341.
Balke, T., T. J. Bouma, E. M. Horstman, E. L. Webb, P. L. A. Erftemeijer, and P. M. J. Herman (2011), Windows of opportunity: Thresholds to mangrove seedling establishment on tidal flats, *Mar. Ecol. Prog. Ser.*, 440, 1–9.

Balke, T., T. J. Bouma, P. M. J. Herman, E. M. Horstman, C. Sudtongkong, and E. L. Webb (2013), Cross-shore gradients of physical disturbance in mangroves: Implications for seedling establishment, *Biogeosciences*, *10*(8), 5411–5419, doi:10.5194/bg-10-5411-2013.

Balke, T., P. M. J. Herman, and T. J. Bouma (2014), Critical transitions in disturbance-driven ecosystems: Identifying Windows of Opportunity for recovery, *J. Ecol.*, *102*, 700–708.

Bearman, J. A., C. T. Friedrichs, B. E. Jaffe, and A. C. Foxgrover (2010), Spatial trends in tidal flat shape and associated environmental parameters in South San Francisco Bay, *J. Coastal Res.*, *26*(2), 342–349.

Booij, N., R. C. Ris, and L. H. Holthuijsen (1999), A third-generation wave model for coastal regions 1. Model description and validation, *J. Geophys. Res.*, *104*, 7649–7666, doi:10.1029/98JC02622.

Bouma, T. J., et al. (2014), Identifying knowledge gaps hampering application of intertidal habitats in coastal protection: Opportunities & steps to take, *Coastal Eng.*, *87*, 147–157, doi:10.1016/j.coastaleng.2013.11.014.

Briggs, W., V. Henson, and S. McCormick (2000), *A Multigrid Tutorial*, 2nd ed., Soc. for Ind. and Appl. Math., Philadelphia, Pa.

Callaghan, D. P., T. J. Bouma, P. Klaassen, D. van der Wal, M. J. F. Stive, and P. M. J. Herman (2010), Hydrodynamic forcing on salt-marsh development: Distinguishing the relative importance of waves and tidal flows, *Estuarine Coastal Shelf Sci.*, *89*(1), 73–88.

Corenblit, D., A. C. W. Baas, G. Bornette, J. Darrozes, S. Delmotte, R. A. Francis, A. M. Gurnell, F. Julien, R. J. Naiman, and J. Steiger (2011), Feedbacks between geomorphology and biota controlling Earth surface processes and landforms: A review of foundation concepts and current understandings, *Earth Sci. Rev.*, *106*(3-4), 307–331, doi:10.1016/j.earscirev.2011.03.002.

D'Alpaos, A., S. Lanzoni, S. M. Mudd, and S. Fagherazzi (2006), Modeling the influence of hydroperiod and vegetation on the cross-sectional formation of tidal channels, *Estuarine Coastal Shelf Sci.*, *69*(3-4), 311–324.

Dissanayake, D. M. P. K., R. Ranasinghe, J. A. Roelvink, and Z. B. Wang (2011), Process-based and semi-empirical modelling approaches on tidal inlet evolution, *J. Coastal Res.*, (Spec. Issue 64), 1013–1017.

Fagherazzi, S., L. Carniello, L. D'Alpaos, and A. Defina (2006), Critical bifurcation of shallow microtidal landforms in tidal flats and salt marshes, *Proc. Natl. Acad. Sci. U.S.A.*, *103*(22), 8337–8341.

Fagherazzi, S., et al. (2012), Numerical models of salt marsh evolution: Ecological, geomorphic, and climatic factors, *Rev. Geophys.*, *50*, RG1002, doi:10.1029/2011RG000359.

Fan, D., Y. Guo, P. Wang, and J. Z. Shi (2006), Cross-shore variations in morphodynamic processes of an open-coast mudflat in the Changjiang Delta, China: With an emphasis on storm impacts, *Cont. Shelf Res.*, *26*(4), 517–538.

Friedrichs, C. T. (2011), Tidal flat morphodynamics: A synthesis, in *Treatise on Estuarine and Coastal Science*, edited by E. Wolanski and D. McLusky, chap. 3.06, pp. 137–170, Academic Press, Waltham, Mass.

Friedrichs, C. T., and D. G. Aubrey (1996), Uniform bottom shear stress and equilibrium hyposometry of intertidal flats, in *Coastal and Estuarine Studies*, vol. 50, edited by C. Pattiaratchi, pp. 405–429, AGU, Washington, D. C.

Friedrichs, C. T., and L. D. Wright (2004), Gravity-driven sediment transport on the continental shelf: Implications for equilibrium profiles near river mouths, *Coastal Eng.*, *51*(8–9), 795–811.

Galappatti, G., and C. B. Vreugdenhil (1985), Depth-integrated model for suspended sediment transport, *J. Hydraul. Res.*, *23*(4), 359–377.

Gong, Z., Z. Wang, M. J. F. Stive, C. Zhang, and A. Chu (2012), Process-based morphodynamic modeling of a schematized mudflat dominated by a long-shore tidal current at the central Jiangsu coast, China, *J. Coastal Res.*, *28*, 1381–1392, doi:10.2112/JCOASTRES-D-12-00001.1.

Green, M. O. (2011), Very small waves and associated sediment resuspension on an estuarine intertidal flat, *Estuarine Coastal Shelf Sci.*, *93*(4), 449–459.

Green, M. O., and G. Coco (2014), Review of wave-driven sediment resuspension and transport in estuaries, *Rev. Geophys.*, *52*, 77–117, doi:10.1002/2013RG000437.

Han, Q., T. J. Bouma, F. G. Brun, W. Suykerbuyk, and M. M. Van Katwijk (2012), Resilience of Zostera noltii to burial or erosion disturbances, *Mar. Ecol. Prog. Ser.*, *449*, 133–143, doi:10.3354/meps09532.

Hasselmann, K. et al. (1973), Measurements of wind-wave growth and swell decay during the Joint North Sea Wave Project (JONSWAP).

Hu, Z., W. Lenting, D. van der Wal, and T. J. Bouma (2015), Continuous monitoring of short-term bed-level dynamics on an intertidal flat: Introducing a novel stand-alone high-resolution SED-sensor, *Geomorphology*, doi:10.1016/j.geomorph.2015.05.027, in press.

Hunt, S., K. R. Bryan, and J. C. Mullarney (2015), The influence of wind and waves on the existence of stable intertidal morphology in meso-tidal estuaries, *Geomorphology*, *228*, 158–174, doi:10.1016/j.geomorph.2014.09.001.

Kirby, R. (2000), Practical implications of tidal flat shape, *Cont. Shelf Res.*, *20*(10–11), 1061–1077.

Kirwan, M. L., and J. P. Megonigal (2013), Tidal wetland stability in the face of human impacts and sea-level rise, *Nature*, *504*(7478), 53–60, doi:10.1038/nature12856.

Kirwan, M. L., G. R. Guntenspergen, A. D'Alpaos, J. T. Morris, S. M. Mudd, and S. Temmerman (2010), Limits on the adaptability of coastal marshes to rising sea level, *Geophys. Res. Lett.*, *37*, L23401, doi:10.1029/2010GL045489.

Kragtwijk, N. G., T. J. Zitman, M. J. F. Stive, and Z. B. Wang (2004), Morphological response of tidal basins to human interventions, *Coastal Eng.*, *51*(3), 207–221, doi:10.1016/j.coastaleng.2003.12.008.

Lanzoni, S., and A. D'Alpaos (2015), On funneling of tidal channels, *J. Geophys. Res. Earth Surf.*, *120*, 433–452, doi:10.1002/2014JF003203.

Le Hir, P., W. Roberts, O. Cazaillet, M. Christie, P. Bassoullet, and C. Bacher (2000), Characterization of intertidal flat hydrodynamics, *Cont. Shelf Res.*, *20*(12-13), 1433–1459.

Lesser, G. R., J. A. Roelvink, J. A. T. M. van Kester, and G. S. Stelling (2004), Development and validation of a three-dimensional morphological model, *Coastal Eng.*, *51*(8–9), 883–915, doi:10.1016/j.coastaleng.2004.07.014.

Liu, X. J., S. Gao, and Y. P. Wang (2011), Modeling profile shape evolution for accreting tidal flats composed of mud and sand: A case study of the central Jiangsu coast, China, *Cont. Shelf Res.*, *31*(16), 1750–1760, doi:10.1016/j.csr.2011.08.002.

Mariotti, G., and S. Fagherazzi (2010), A numerical model for the coupled long-term evolution of salt marshes and tidal flats, *J. Geophys. Res.*, *115*, F01004, doi:10.1029/2009JF001326.

Murray, A. B., M. A. F. Knaapen, M. Tal, and M. L. Kirwan (2008), Biomorphodynamics: Physical-biological feedbacks that shape landscapes, *Water Resour. Res.*, *44*, W11301, doi:10.1029/2007WR006410.

Pritchard, D., and A. J. Hogg (2003), Cross-shore sediment transport and the equilibrium morphology of mudflats under tidal currents, *J. Geophys. Res.*, *108*(10), 3313, doi:10.1029/2002JC001570.

Pritchard, D., A. J. Hogg, and W. Roberts (2002), Morphological modelling of intertidal mudflats: The role of cross-shore tidal currents, *Cont. Shelf Res.*, *22*(11–13), 1887–1895.

Roberts, W., P. Le Hir, and R. J. S. Whitehouse (2000), Investigation using simple mathematical models of the effect of tidal currents and waves on the profile shape of intertidal mudflats, *Cont. Shelf Res.*, *20*(10–11), 1079–1097.

Roelvink, J. A., and A. J. H. M. Reniers (2011), *A Guide to Modelling Coastal Morphology*, World Sci. Co., Singapore.

Rossington, S. K., R. J. Nicholls, M. J. F. Stive, and Z. B. Wang (2011), Estuary schematisation in behaviour-oriented modelling, *Mar. Geol.*, *281*(1–4), 27–34, doi:10.1016/j.margeo.2011.01.005.

Soulsby, R. L. (1995), Bed shear-stresses due to combined waves and currents, in *Advances in Coastal Morphodynamics*, edited by M. J. F. Stive et al., pp. 4-20–4-23, Delft Hydraul., Delft, Netherlands.

Stive, M. J. F., and Z. B. Wang (2003), Morphodynamic modeling of tidal basins and coastal inlets, in *Elsevier Oceanography Series*, vol. 67, edited by V. C. Lakhan, chap. 13, pp. 367–392, Elsevier, Amsterdam.

Stive, M. J. F., Z. B. Wang, M. Capobianco, P. Ruol, and M. C. Buijsman (1998), Morphodynamics of a tidal lagoon and the adjacent coast, in *Physics of Estuaries and Coastal Seas: Proceedings of the 8th International Biennial Conference on Physics of Estuaries and Coastal Seas, The Hague, Netherlands*, edited by J. Dronkers and M. Scheffers, pp. 397–407, AA Balkema, Rotterdam, Netherlands.

Tambroni, N., and G. Seminara (2012), A one-dimensional eco-geomorphic model of marsh response to sea level rise: Wind effects, dynamics of the marsh border and equilibrium, *J. Geophys. Res.*, *117*, F03026, doi:10.1029/2012JF002363.

Temmerman, S., P. Meire, T. J. Bouma, P. M. J. Herman, T. Ysebaert, and H. J. De Vriend (2013), Ecosystem-based coastal defence in the face of global change, *Nature*, *504*(7478), 79–83, doi:10.1038/nature12859.

Tucker, M. J., and E. G. Pitt (2001), *Waves in Ocean Engineering*, 1st ed., Elsevier, Amsterdam, New York.

Van der Wegen, M., and B. E. Jaffe (2014), Processes governing decadal-scale depositional narrowing of the major tidal channel in San Pablo Bay, California, USA, *J. Geophys. Res. Earth Surf.*, *119*, 1136–1154, doi:10.1002/2013JF002824.

Van Goor, M. A., T. J. Zitman, Z. B. Wang, and M. J. F. Stive (2003), Impact of sea-level rise on the morphological equilibrium state of tidal inlets, *Mar. Geol.*, *202*(3–4), 211–227, doi:10.1016/S0025-3227(03)00262-7.

Van Kessel, T., J. Vanlede, and J. de Kok (2011), Development of a mud transport model for the Scheldt estuary, *Cont. Shelf Res.*, *31*(10 Suppl.), S165–S181, doi:10.1016/j.csr.2010.12.006.

van Rijn, L. C. (1993), *Principles of Sediment Transport in Rivers, Estuaries and Coastal Seas*, p. 3.13, Aqua Publ., Amsterdam.

Van Rijn, L. C. (2007a), Unified view of sediment transport by currents and waves. I: Initiation of motion, bed roughness, and bed-load transport, *J. Hydraul. Eng.*, *133*(6), 649–667, doi:10.1061/(ASCE)0733-9429(2007)133:6(649).

Van Rijn, L. C. (2007b), Unified view of sediment transport by currents and waves. II: Suspended transport, *J. Hydraul. Eng.*, *133*(6), 668–689, doi:10.1061/(ASCE)0733-9429(2007)133:6(668).

Waeles, B., P. Le Hir, and R. Silva Jacinto (2004), Cross-shore morphodynamical modelling of an intertidal mudflat, *C. R. Geosci.*, *336*(11), 1025–1033.

Wang, Z. B., and I. H. Townend (2012), Influence of the nodal tide on the morphological response of estuaries, *Mar. Geol.*, *291–294*, 73–82, doi:10.1016/j.margeo.2011.11.007.

Wang, Z. B., B. Karssen, R. J. Fokkink, and A. Langerak (1998), A dynamic-empirical model for estuarine morphology, in *Physics of Estuaries and Coastal Seas: Proceedings of the 8th International Biennial Conference on Physics of Estuaries and Coastal Seas, The Hague, Netherlands*, edited by J. Dronkers and M. Scheffers, pp. 279–286, AA Balkema, Rotterdam, Netherlands.

Wang, Z. B., H. de Vriend, M. Stive, and I. Townend (2008), On the parameter setting of semi-empirical long-term morphological models for estuaries and tidal lagoons, in *River, Coastal and Estuarine Morphodynamics: RCEM 2007, Two Volume Set*, pp. 103–111, Taylor & Francis, London.

Winterwerp, J. C., and W. G. Van Kesteren (2004), *Introduction to the Physics of Cohesive Sediment Dynamics in the Marine Environment*, *Dev. in Sedimentol.*, vol. 56, Elsevier, Amsterdam.

Zhu, Q., S. Yang, and Y. Ma (2014), Intra-tidal sedimentary processes associated with combined wave–current action on an exposed, erosional mudflat, southeastern Yangtze River Delta, China, *Mar. Geol.*, *347*, 95–106, doi:10.1016/j.margeo.2013.11.005.